Chapter 5

HYBRID 2D/0D SnS_2 NANOFLAKES/CTS QDs-BASED BROADBAND (UV-VISIBLE-NIR) PHOTODETECTOR

This chapter report the fabrication and characterization of 2D/0D SnS_2 nanoflakes/CTS QDs based UV-Visible-NIR range photodetector. In this chapter we have improved the performance of the photodetector in comparison to the photodetection structures discussed in Chapter-2, 3 and 4 by combining SnS_2 nanaoflakes with CTS QDs. This chapter shows the improvement in optical performance and extension of bandwidth compared to earlier reported works in the previous chapters. In this chapter the absorption of both active materials has been utilized to achieve a broadband photodetection structure. Here, SnS_2 nanaoflakes work as active materials for UV radiation while CTS QDs absorb light in Visible-NIR regions and realize a efficient broadband photodetection structure [*]

[*]Parts of this chapter have been published in Sanjeev Mani Yadav, and Amritanshu Pandey. "Hybrid 2D–0D SnS_2 Nanoflakes/CTS QDs-Based Broadband (UV-Visible-NIR) Photodetector." *IEEE Transactions on Electron Devices* 67.5 (2020): 2008-2015.

5.1 Introduction

Photodetectors (PDs) are broadly classified as broadband or selective on the basis of their spectrum detection capability. PDs with broad light detection/sensing capabilities have variety of applications such as imaging, remote sensing, spectroscopy and optical fibre communication [194, 311]. The most challenging factor for broadband photodetectors are the selection of materials with broad light absorption capability, high mobility, and high stability. These properties are correspondingly attributed to wide bandwidth, fast, and stable operation of PDs. Popularly used semiconductors for the fabrication of photodetector devices have its best operating performances either in UV or in visible or NIR bands e.g., GaN, Si, InGaAs are used to detect the light in the wavelength range of UV (0.25—0.4 μm), visible (0.45—0.8 μm) and NIR (0.9—1.7 μm), respectively [312, 28]. The band gap property of such bulk materials cannot be tuned hence, researchers are attracted towards low dimensional materials having the band gap tunability by varying its nanoscale dimensions [313]. Variety of photodetectors has been reported based on 2-dimensional (2D) semiconductors such as graphene, WS_2, MoS_2, $MoSe_2$ etc. [314]

Graphene, a ultra high mobility material with single layered mobility in the order of $\sim 10^5$ $cm^2/V\text{-}s$ and having zero bandgap, has been explored widely for high speed and wideband photodetection [315, 191]. However, graphene PDs have poor responsivity due to very small absorption (2.3%) [191]. Further, costly fabrication techniques with non uniform resultant graphene layer have also limited its application for high performance wideband PDs. Significant improvement in detection characteristics of graphene based PD are obtained by stacking it with some other materials and nano-structures but at the cost of fabrication complexity [316, 23, 191, 317].

Transition metal dichalcogenides (TMDs) such as WS_2, MoS_2, $MoSe_2$ with moderate mobility and high absorption coefficients, [95] have also been explored for superior responsivity broadband photodetection [318, 319] although, their low band gap tunability (1–2 eV) limit their operation in visible or vis-NIR sub-bands only [100].

SnS_2, a member of layered metal dichalcogenide (LMDs) family, is a promising can-

didate for PDs. It has high absorption coefficient 10^4 cm^{-1} and mobility 230 cm^2/V-s at room temperature [103, 119]. Further SnS_2, is a nontoxic, environment-friendly, chemically stable, abundant, large bandgap, n-type 2D semiconductor material, belonging to CdI_2–type structure [102, 103, 119]. The SnS_2 nano-flakes/sheets exhibit strong absorption in UV-vis band but poor absorption in NIR region [320, 96]. The poor absorption of SnS_2 in NIR region can be enhanced by combining it with some other nanostructures to facilitate broadband detection with improved optical characteristics. Usually quantum dots (0D) are used for such purpose due to their high surface to volume ratio which leads high absorption of light. The quantum dots of PbS, HgTe etc., reported with their strong absorption in NIR regions [127, 128], are good candidate to form hybrid with SnS_2 for broadband detection with high responsivity and detectivity. The toxicity of PbS, Hg and rarity of Te material leads to look for the substitution of these QDs by a nontoxic material having optical absorption in NIR region.

Cu_2SnS_3 (CTS), a p-type semiconductor having large absorption coefficient (>10^4 cm^{-1}) fulfills the above requirement in term of its non-toxicity, earth-abundant and strong absorption for NIR regions [5]. Furthermore, CTS QDs have large band gap tunability (0.93- 1.77 eV) [5] depending on its size.

Accordingly, this chapter reports a SnS_2 nanoflakes-CTS QDs (2D-0D) hybrid photodetector for broadband operation in UV-Vis-NIR region of spectrum. Both of the active materials have been synthesized by low cost solvothermal method. The absorption spectra of both materials in their respective regions are confirmed by absorption spectrum measured for broad range (300-1100 nm). The electrical and optical characteristics of the fabricated device, such as sensitivity, responsivity, detectivity and EQE, are also measured to confirm the advantage of the 2D-0D hybrid PD compared to other reported broadband photodetectors.

5.2 Experimental Details

5.2.1 Solvothermal Synthesis of SnS_2 Nanoflakes

The solvothermal synthesis of SnS_2 have been carried out as per the technique discussed in literature [321]. In brief, the synthesis of SnS_2 nano flakes have been done by taking 1-mmol of $SnCl_4.5H_2O$ and 2.5-mmol of thiourea (CH_4N_2S) in 30 ml of ethylene glycol. The resultant solution was magnetic stirred and ultrasonicated till the homogeneous and transparent solution was obtained. In the next step, the resultant transparent solution was placed in 50 ml Teflon-lined autoclave at temperature of 180°C for $\sim$24 h. After cooling at room temperature, the resultant yellowish solution of SnS_2 nanoflakes are collected and used for the structural and optical characterization and for device fabrication.

5.2.2 Solvothermal Synthesis of CTS QDs

The solvothermal synthesis of CTS QDs have been performed by making a solution of 0.3 mmol of $SnCl_2.2H_2O$, 0.62 mmol of $CuCl_2.2H_2O$ and 1.6 M PVP (M_w = 2.5 g mol^{-1}) in 20 ml of ethylene glycol. A second solution of 0.93 mmol of Na_2S was prepared in 20 mL of ethylene glycol as per the reports [23, 5]. Now, the prepared solution of Na_2S in ethylene glycol was added drop wise in the first solution along with magnetic stirring. The resultant homogeneous brownish black solution was then transferred to a 50 ml autoclave and kept at 180°C for $\sim$12 h. The product obtained was washed several times with DI water to remove the organic impurities and then it was dried in vacuum. The resultant brownish powder is CTS QDs.

5.2.3 Device Fabrication Steps

5.2.3.1 Substrates Cleaning

This process includes the cleaning of p-Si (100) substrates of resistivity 2–7 ohm-cm by standard process. In brief, the Si substrates have been ultrasonically treated in

TCE solution followed by acetone for 10 min each. The resultant substrates were then rinse in DI water for 5-6 times. In next step the substrates were dip in the solution of H_2O_2:H_2SO_4 (60:40) for 15 min and then by rinse with DI water for several times. In final step the resultant substrates were dip in the solution of HF:DI (10:60) for 10 min and then rinse with DI water several times followed by hot air oven dry.

5.2.3.2 Oxidation of Si Substrate

This growth of SiO_2 layer of thickness ∼300 nm over cleaned Si substrate was done by performing dry, wet and dry oxidation, for ∼10, ∼13, and ∼10 min, respectively at the furnace temperature of 1100°C.

5.2.3.3 Transferring SnS_2 Nanoflakes on SiO_2/Si Substrate

Through this process the SnS_2 nanoflakes were coated over SiO_2/Si substrate using spin coating technique. Few drops of the synthesized SnS_2 solution were released using micropipette on SiO_2/Si substrate followed by the rotation of substrate at 2000 r.p.m.for 20 sec, and then dried for 3 min at ∼130°C. The above coating and drying processes were repeated for 5 times to obtain a uniform and multiple layers of SnS_2 over SiO_2/Si substrate.

5.2.3.4 Metal Contact Formation on SnS_2 Nanoflakes/SiO_2/Si Structure

Multiple Ag metal contacts of thickness ∼90 nm thickness and 2 mm in diameter are patterned on SnS_2 nanoflakes/SiO_2/Si structure as shown in Fig.5.1 (b). In this process, Ag material (purity (99.99%)) is vacuum evaporated in thermal coating unit (Model-BC-300) and patterned on SnS_2 nanoflakes/ SiO_2/Si structure using shadow masking technique. The obtained silver patterned device was then annealed at ∼120°C for ∼4 min under the ambient environment. The annealing of the device is performed to improve the adhesiveness of Ag over SnS_2 nanoflakes as well as to improve (reduce) the contact resistance between SnS_2 nanoflakes and Ag electrodes.

5.2.3.5 Drop Casting of CTS QDs over SnS_2 Nanoflakes/SiO_2/Si Structure

In the final step of device fabrication, 50 mg of synthesized CTS QDs are dispersed in 1 ml of ethanol solution and ∼80 μl of this uniformly dispersed solution was drop casted over Ag patterned SnS_2 nanoflakes/ SiO_2/Si structure with the help micropipette and then dried. The resultant CTS QDs/SnS_2 nanoflakes based photodetector structure is shown in Fig.5.1.

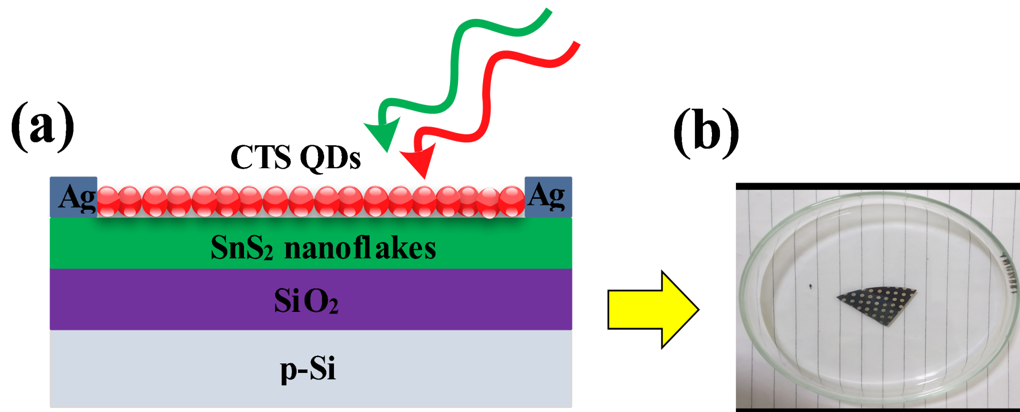

Figure 5.1: (a) Schematic of proposed device structure, (b) Fabricated broadband photodetectors under consideration

5.3 Result and Discussion

5.3.1 Structural Characterization of SnS_2 Nanoflakes

The X-ray diffraction (XRD) pattern of synthesized SnS_2 nanoflakes over SiO_2/p-Si(100) substrate are performed by Rigaku smart lab 9 kW equipped with a Cu K-α source of 1.5405 Å) for 2θ ranges from 10° to 80° (Fig.5.2 (a)). The XRD pattern is well matched with JCPDS 023-0677 data and confirm the hexagonal phase crystal structure of synthesized SnS_2 nanoflakes. The XRD pattern shows the multiple high intense peaks. The highest intensity peaks of solvothermal synthesized SnS_2 nanoflakes are observed for (001), (100), (110) and (201) plane orientations confirming that these plane orientations are predominate.

The Raman spectra of SnS_2 nanoflakes was recorded to confirm the structural fingerprint and vibrations modes of molecules by using Raman Spectrophotometer with laser excitation of 532 nm. The Raman spectra shows a peak at 312.15 cm^{-1} which corresponds to the A_{1g} vibration mode of 2H-SnS_2 [322] as shown in Fig.5.2 (b). The molecular vibration mode of SnS_2 along with atomic arrangement are given in inset of Fig.5.2 (b).

The field emission scanning electron microscopy (FE-SEM) image of the synthesized SnS_2 nanoflakes recorded by Nova Nano SEM 450, FEI Company of USA (S.E.A.) is shown in Fig.5.2 (c). The high-resolution FE-SEM image confirm the presence of SnS_2 nanoflakes and their morphology over larger surface area.

The transmission electron microscopy (TEM) of the synthesized SnS_2 was performed by Tecnai G2 20 TWIN, FEI Company of USA (S.E.A.) to measure the size of nanoflakes. The various size of the nanoflakes approximated with hexagonal shapes have been recorded in the ranges of 90-190 nm as marked in Fig.5.2 (d). The distribution of nanoflakes against their dimensions are also presented by the histogram plot in Fig.5.2 (e). The average size of the synthesized nanoflakes is estimated to be ~146 nm which matches well with the range of SnS_2 nanoflakes dimensions reported in literature [323]. The selected area electron diffraction (SAED) pattern of SnS_2 nanoflakes are shown in Fig.5.2 (f). The clear and bright circular rings along with corresponding planes observed in SAED pattern confirm the highly crystalline geometry of SnS_2 nanoflakes.

5.3.2 Structural Characterization of CTS QDs

The TEM images of synthesized CTS QDs at two different scales as shown in Fig.5.3 (a) and (b), clearly show the clusters of CTS QDs and confirm the presence of QDs of various sizes as marked by circles. The size distribution of the QDs are also realized by making a histogram of recorded particle sizes. The average size of CTS QDs is estimated to be ~3.2 nm which is smaller than the Bohr radius of CTS [68]. The smaller size of our synthesized CTS QDs with respect to Bohr's radius leads strong confinement effects. Fig.5.3 (c) shows the HR-TEM image of CTS QDs along with its corresponding

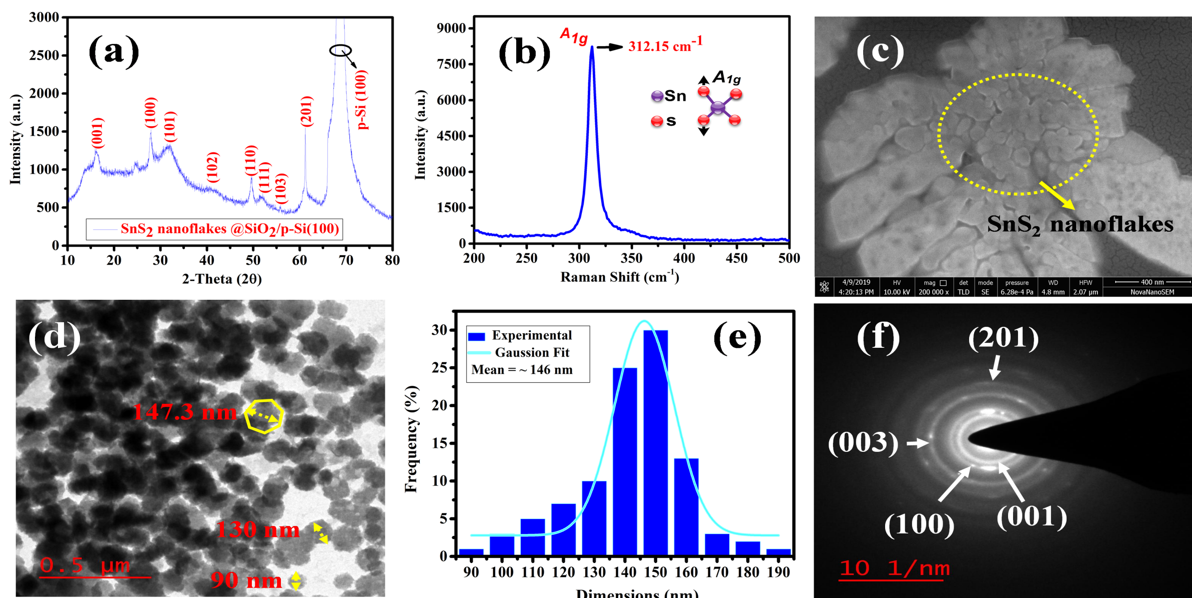

Figure 5.2: (a) XRD of solvothermal synthesized SnS_2 nanoflakes, (b) Raman spectra of SnS_2 nanoflakes with marked vibration mode (A_{1g}) and its atomic representation, (c) FE-SEM image of SnS_2 nanoflakes at high magnification scale, (d) TEM image of SnS_2 nanoflakes along with marked dimensions, (e) Histogram plot relating nanoflakes dimensions with their occurrence frequencies to estimate the average size of nanoflakes by Gaussian approximation and, (f) SAED pattern of solvothermal synthesized SnS_2 nanoflakes to insure the crystalline geometry

SAED pattern to confirm structural geometry. Further, HR-TEM image with marked inter-planar spacing and their corresponding plane are also shown in Fig.5.3 (c) which are matched well with structural geometrical data of CTS QDs.

5.3.3 Structural Characterizations of the Hybrid CTS QDs/SnS_2 Nanoflakes Based Structure

The Atomic Force Microscopy (AFM) of SnS_2 nanoflakes (Fig.5.4 (a)) and CTS QDs/SnS_2 nanoflakes over SiO_2/Si substrate (Fig.5.4 (b)) was performed by NTEGRA Prima, NT-MDT Service & Logistics Ltd. to confirm the presence and corresponding morphology of SnS_2 nanoflakes and CTS QDs. This obtained AFM image confirms the presence of SnS_2 nanoflakes with maximum height of ~15 nm as per height scale bar (Fig.5.4 (a)). Fig.5.4 (b) shows the AFM image of CTS QDs over SnS_2 nanoflakes/SiO_2/Si structure. This AFM image confirms the presence of agglomerated CTS QDs over SnS_2 nanoflakes

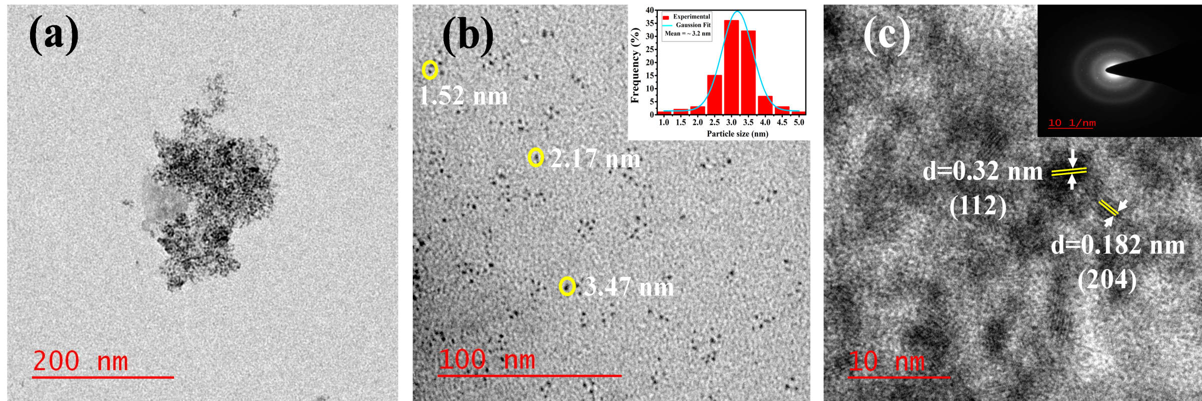

Figure 5.3: (a) TEM image of CTS QDs at 200 nm scale, (b) TEM image of CTS QDs with their estimated dimension along with their size distribution histogram plot inset, (c) HR-TEM image of CTS QDs with plane indexing and the SAED pattern of corresponding HR-TEM image inset

marked with circle; while the brighter portions in image confirm the presence of SnS_2 nanoflakes.

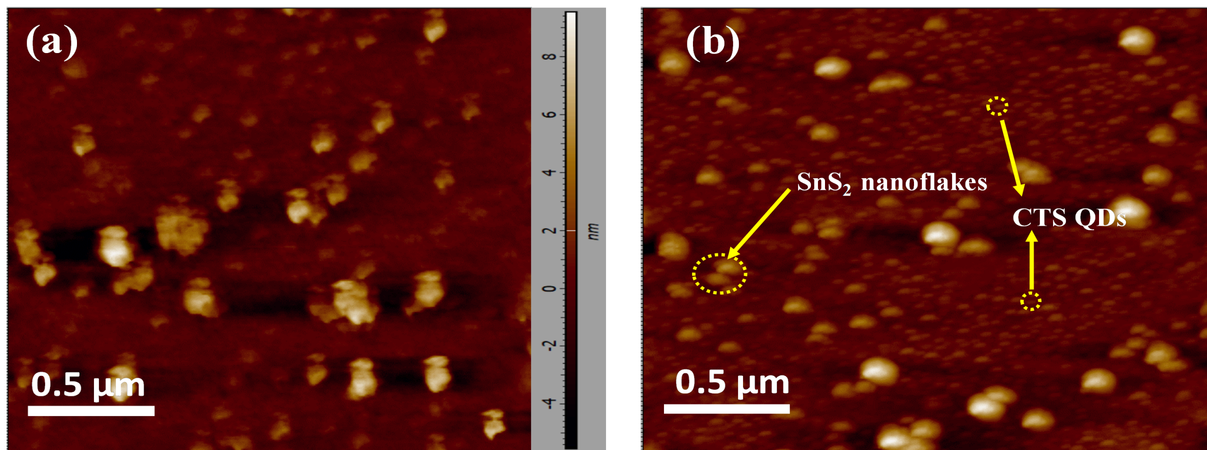

Figure 5.4: (a) AFM image of SnS_2 nanoflakes over SiO_2/Si substrate, (b) AFM image of agglomerated CTS QDs over SnS_2 nanoflakes/ SiO_2/Si structure.

5.3.4 Electrical and Optical Characterization of Fabricated Device

The performance parameters of fabricated PD based on CTS QDs/SnS_2 nanoflakes has been carried out with the help of current density–voltage, and current-wavelength measurements. The J-V response of the device under dark condition, shown in Fig.5.5 (a),

is done with the help of the parameter analyser at various applied voltages. Further, the performance of the fabricated device under light illumination with broad-spectrum (300-1100 nm wavelengths) has been performed by using a light source along with monochromator, and a digital multimeter at various applied voltages. The monochromator facilitates single wavelength light to illuminate the device while digital meter was used to record the current levels for each illuminated wavelength under broad spectrum ranges (300—1100 nm) for a fixed bias. The fabricated device portrays huge photocurrent for incident UV-Vis-NIR (300-1100 nm) lights. These high current density levels of the device for UV-Vis-NIR spectrum light are attributed to the strong light absorption of SnS_2 nanoflakes and CTS QDs in UV and Vis-NIR region, respectively; as confirmed by their absorption spectra (Fig.5.5 (c)). The absorption spectra of SnS_2 nanoflakes clearly show a strong absorption for UV region whereas the absorption of the nanoflakes is small towards Vis-–NIR regions in agreement to the reports [105, 188]. Hence to achieve the broadband detection from a SnS_2 nanoflakes based photodetector, a hybrid of SnS_2 nanoflakes and CTS QDs having strong absorption in NIR spectrum, (Fig.5.5 (c)) is proposed. The photo-current to dark-current ratio (sensitivity) of the detector for the hybrid SnS_2 nanoflakes/CTS QDs are found to be 296.2, 240.7 and 368.05 for 320, 640 and 970 nm illumination wavelengths, respectively at 5 V. The observed sensitivity of the CTS QDs/SnS_2 nanoflakes based detector is found to be comparable and better than that of many broadband photodetectors reported in the literature [105, 23, 213, 63]. Further, the current density-–wavelength spectra of the device is affected by operating voltage i.e., the current density at 5 V are observed to be ∼50 times more than the current density observed at 2.5 V.

The other optical characteristics of CTS QDs/SnS_2 nanoflakes based device like responsivity (R), EQE and detectivity (D) are calculated by (5.1), (5.2) and (5.3), respectively [324].

$$Responsivity(R) = \frac{J_p}{P_{opt}} \tag{5.1}$$

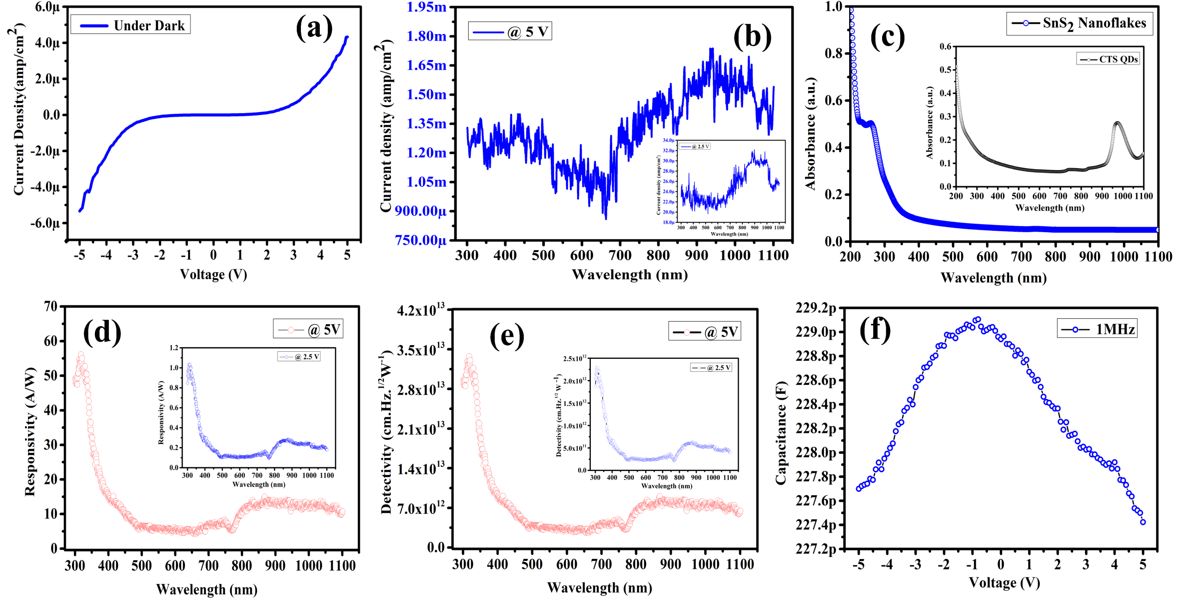

Figure 5.5: (a) Current density–voltage characteristics under dark condition, (b) Current density variation with respect to illumination light wavelength at 5 V and 2.5 V (Inset), (c) Absorption spectra of SnS_2 nanoflakes along with absorption spectra of CTS QDs (Inset), (d) Responsivity of the device at various wavelength with applied bias 5 V and 2.5 V, (e) Detectivity of the device at various wavelength with applied bias 5 V and 2.5 V, (f) C-V characteristics of the fabricated device at 1-MHz

$$EQE(\eta) = \frac{hc}{\lambda q} R =\sim \frac{1240}{\lambda(nm)} R \tag{5.2}$$

$$Detectivity(D) = \frac{\lambda \eta q}{hc} \sqrt{\frac{RA}{4kT}} \tag{5.3}$$

where, J_P is the photocurrent density and P_{opt} is the optical power density of the illuminated light. Further in (3) the ratio q$\eta\lambda$/hc denotes the responsivity (R) of the device in term of external quantum efficiency (η), (RA) is the resistance area product and defined as $RA = (\partial \mathrm{J}/\partial \mathrm{V})^{-1} = kT/qJ$.

The responsivity of the device for the applied voltages of 2.5 V and 5 V are shown in Fig.5.5 (d). The device shows good responsivity in entire range with the highest responsivity for UV and NIR region while it is minimum for visible region ∼(500-650 nm). The responsivity of the device are found to be 53.88 and 12.61 (A/W) for 320 and 970 nm illumination wavelengths respectively for 5 V applied bias, while the responsivity

for 640 nm light illumination are found to be ~5 (A/W). Similarly, responsivity of the device has also been measured at 2.5 V for the same optical power intensity and is found to be ~1, 0.11 and 0.22 (A/W) for 320, 640, 970 nm illumination wavelengths, respectively. The EQE of the device is also calculated as per (2) and found to be 208.78, 9.99, 16.12 for 320, 640 and 970 nm illumination wavelengths, respectively at 5 V applied bias.

The detectivity of the device is dependent of dark current and responsivity. The dark current of the proposed device changes drastically as the voltage changes from 2.5 to 5 V (shown in Fig.5.5 (a)) therefore degrade the detectivity of the device at higher voltage. The calculated detectivity of the device under 2.5 V and 5 V is shown in Fig.5.5 (e). The highest detectivity of the device, for applied bias 2.5 V and 5 V are found to be the order of $\sim 10^{12}$ and $\sim 10^{13}$ (Jones) respectively for 320 nm illumination wavelength. The small change in capacitance with respect to applied voltage is observed in the proposed device as evident from C-V plot at 1-MHz frequency (shown in Fig.5.5 (f)), demonstrating the charge storing capability of the device (C=dQ/dV).

The obtained responsivity, EQE, and detectivity of this device for broad spectrum region with low illumination optical power density are found to be much better and comparable than the other reported broadband photodetectors [105, 213, 23, 325, 317, 63]. The strong optical characteristics of the device make it suitable candidate for broadband application like bio-imaging, remote sensing, and in the field of optical communication etc. [326] The obtained optical characteristics of the device have been summarized in Table-5.1. A comparative analysis of the fabricated photodetector with some other reported photodetectors has been summarized in Table-II. The optical characteristics of the fabricated device are found to be comparable and better than the other reports in the context of broadband detection.

5.4 Principle of Operation

The carrier transportation mechanism between Ag/n-SnS_2/Ag and n-SnS_2/p-CTS QDs in the fabricated PD device (Fig.5.6 (a)) may be explained with the help of band

Table 5.1: Comparison Table With Some Other Reported Photodetectors

Parameters	**This work**	**[105]**	**[23]**	**[213]**	**[325]**	**[317]**	**[63]**
Device structure	CTS QDs/SnS_2 nanosheet	SnS_2 nanoflakes	CTS QDs/Graphene	Au/SnS nanoflakes	SWCNT/PbS-QDs/PE	Graphene/ ZnO/silicon	Ag/CTS thin-film
Applied Bias (V)	5	5	4.5	5	1	-2	3
Wavelength (nm)	320, 640, 970	365,650,850	650, 850, 1066	405, 650, 850	500, 980, 1300	——	880,920,1050
Spectral ranges (nm)	300-1100	300-1100	600-1100	450-850	300-1500	350-1200	750-1150
Illumination Intensity (μW/cm^2)	23.74 (@320 nm) 201.53 (@640 nm) 125.88 (@970 nm)	3.87 μW (@365 nm) 0.0592 μW (@650 nm) 0.0678 μW (@850 nm)	202.32 (@650 nm) 108.43 (@850 nm) 123.08 (@1066 nm)	16080 (@405 nm) 28470 (@650 nm) 12110 (@850 nm)	13 (@980 nm)	(0–171 mW)	——-
Sensitivity	296.2 (@320 nm) 240.7 (@640 nm) 368.05 (@970 nm)	1.23	7.19 (@650 nm) 7.32 (@850 nm) 7.29 (@1066 nm)	~1.02 (@405 nm) ~1.04 (@650 nm) ~1.39 (@850 nm)	——-	——-	4.32 (@880 nm) 5.47 (@920 nm) 5.74 (@ 1050 nm)
Responsivity (A/W)	53.88 (@320 nm) 5.16 (@640 nm) 12.61 (@ 970 nm)	2.06×10^{-4} (@365 nm) 6.12×10^{-6} (@650 nm) 1.22×10^{-8} (@850 nm)	57.43 (@650 nm) 110.08 (@850 nm) 99.12 (@1066 nm)	0.329 (@405 nm) 0.085 (@650 nm) 0.2027 (@850 nm)	0.5 (@500 nm) 0.006 (@980 nm) 0.35(@1300 nm)	0.2–0.5	10.17m (@880 nm) 13.25m (@920 nm) 10.93m (@1050 nm)
Detectivity (Jones)	3.2×10^{13} (@320 nm) 3.1×10^{12} (@640 nm) 7.5×10^{12} (@970 nm)	——	6.65×10^{11} (@650 nm) 1.25×10^{12} (@850 nm) 1.21×10^{12} (@1066 nm)	1.85×10^{8} (@405 nm) 5.14×10^{7} (@650 nm) 1.22×10^{8} (@850 nm)	1.4×10^{11} (@500 nm) 0.9×10^{11} (@1300 nm)	3.9×10^{13}	3.23×10^{10} (@880 nm) 4.21×10^{10} (@920 nm) 3.47×10^{10} (@1050 nm)
EQE(%)	20878 (@320 nm) 999 (@640 nm) 1612 (@970 nm)	———	10977 (@650 nm) 16090 (@850 nm) 11552 (@1066 nm)	101.08 (@405 nm) 16.37 (@650 nm) 29.59 (@850 nm)	——	——	2.29 (@880 nm) 2.99 (@920 nm) 2.47 (@1050 nm)

diagrams shown in Fig.5.6 (b) and (c), respectively. Under broad light illumination CTS QDs and/or SnS_2 nanoflakes generate photo carriers, which are in turn transferred to the electrodes (Ag) resulting in photocurrent.

The SnS_2 nanoflakes of various sizes play dominant role to absorb the UV photons and generate electron-hole pairs. The generated carriers are collected at Ag electrode and contribute the major current component for this region of operation because the charge carriers in n-SnS_2 do not have any barrier in its journey from n-SnS_2 to Ag contact under any bias (Fig.5.6 (b)). Hence, the SnS_2 layer is responsible for large

carrier generations under UV illumination as well as acts as transport layer to carry these carriers towards electrode. Since CTS QDs have very low absorption of UV light, a negligible contribution of current is achieved in total current. Hence the contribution of this current may be neglected compared to the current obtained by SnS_2 nanoflakes under UV illumination. When visible light ∼(500-650 nm) is incident the resultant current observed in PD is due to contributions of SnS_2 nanoflakes and CTS QDs both. Although the absorption of any one component is not very high, total current observed is significant. Furthermore, when the device is illuminated with NIR radiation CTS QDs play major role and absorb maximum photon energy for this band due to its high absorbance therefore, generate electron hole pair in CTS QDs while SnS_2 nanoflakes having very low absorption for this illumination band do not contribute in photo carriers.

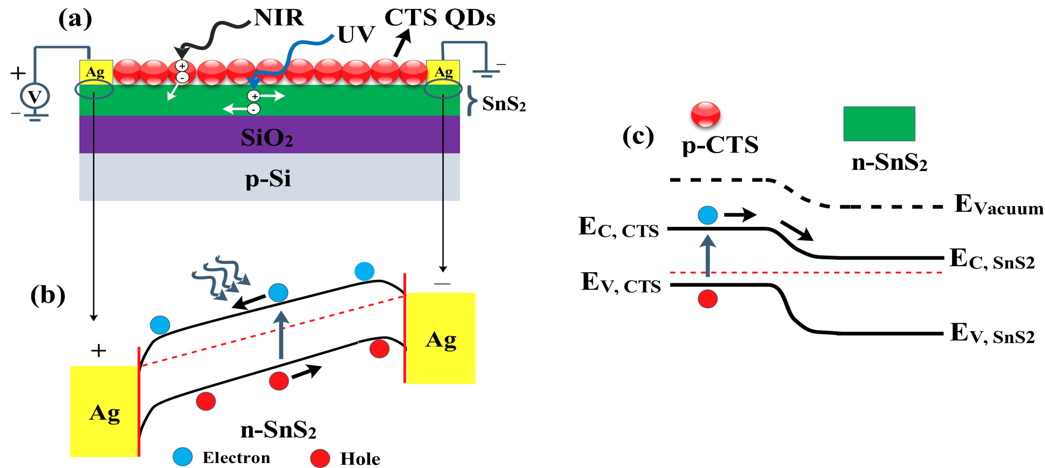

Figure 5.6: (a) Device structure under UV-NIR light illumination, (b) Band energy diagram and charge transportation for Ag/n-SnS_2/Ag structure under thermal equilibrium with an applied bias, (c) Band energy diagram and carriers transportation of between p-CTS QDs and n-SnS_2 nanoflakes under thermal equilibrium

The NIR photogenerated carriers in CTS QDs move under the influence of bias and gets separated thereby reducing the recombination rate significantly. Due to discontinuity of QDs, Ag-CTS QDs-Ag path is less probable [128]. Therefore, the generated holes are trapped in CTS QDs whereas, the electrons move towards SnS_2 nanoflakes channel located below CTS QDs and contribute to large current (Fig.5.6 (c)) [128]. The trapped holes charges in CTS QDs can further oppose the motion of holes from SnS_2 to CTS QDs which will enhance carrier density in SnS_2 channel. The charge carriers

generated in SnS_2 are carried by itself under UV illumination. Hence, the layer SnS_2 acts as transport layer to carry these carriers towards electrode for the electrons generated in CTS QDs also. The fabricated device is also showing large variation in their optical characteristics with respect to applied voltage. The optical characteristics of the device are measured at 2.5 and 5 V applied bias as shown in Fig.5.5 (b), (d) & (e). The small value of optical current density, responsivity and detectivity are reported at 2.5 V, while these parameters improve drastically at higher voltage for example the current density of the device improve ∼50 times as voltage changes front 2.5 to 5 V for broad range of wavelength. Hence the resultant device exhibit good performance for broad spectral range i.e., 300-1100 nm in terms of their optical characteristics at 5 V applied bias.

5.5 Conclusion

In this chapter, we have reported a low cost UV-Vis-NIR broadband photodetector based on nanocomposite structures of 2D-SnS_2 nanoflakes and 0D-CTS QDs to extend the detection ranges of the structures discussed in Chapter-2 and Chapter-4. This chapter concludes the all detection structures discussed so far in Chapter-2, 3 and 4 in term of broadband realization and improved photodetection characteristics. The fabricated hybrid CTS QDs/SnS_2 nanoflakes based photodetector shows excellent optoelectronic properties in UV-Vis-NIR range due to the strong light absorption for these bands by synthesized nanostructures and their high surface to volume ratio. The optical sensitivity of the device for 320, 640 and 970 nm are found to be 296.2, 240.7 and 368.05 respectively at an applied bias 5 V. The responsivity of the device was also measured and found to be 53.88, 5.16 and 12.61 (A/W) for 320, 640, and 970 nm respectively. The observed detectivity of the device is better than many similar type of reported detectors which make this detector very suitable for noisy environment. The fabricated broadband device can be used in broad range of applications like color imaging, bio-sensing, and solar cell etc., due to its broad sensing ability and leads a low cost photodetector.